International Journal of Rock Mechanics & Mining Sciences 64 (2013) 6–16

Contents lists available at ScienceDirect

International Journal of Rock Mechanics & Mining Sciences

journal homepage: www.elsevier.com/locate/ijrmms

Microseismic frequency-spectrum evolutionary rule of rockburst triggered by roof fall

Cai-Ping Lu [a,b,*], Lin-Ming Dou [a], Nong Zhang [a], Jun-Hua Xue [c], Xiao-Nan Wang [a], Hui Liu [a], Jun-Wei Zhang [a]

[a] School of Mining Engineering, Key Laboratory of Deep Coal Resource Mining (Ministry of Education), China University of Mining and Technology, Xuzhou, Jiangsu 221116, PR China

[b] Department of Geosciences and Center for Geomechanics, Geofluids, and Geohazards, Pennsylvania State University, University Park, State College, Pennsylvania 16802, USA

[c] State Key Laboratory of Deep Coal Mining and Environment Protection, Huainan Mining Industry Group, Huainan, Anhui 232001, PR China

ARTICLE INFO

Article history:
Received 26 July 2012
Received in revised form
27 May 2013
Accepted 13 August 2013
Available online 10 September 2013

Keywords:
Rockburst
Roof fall
Frequency-spectrum evolution
Low-frequency precursor
Predominant frequency

ABSTRACT

Strong rockburst disaster in deep coal mines is easily triggered by the higher static stress of mining coal seam and the dynamic stress wave disturbance generated by hard and thick roof fall. Revealing the frequency-spectrum evolutionary rule of microseismic (MS) signals before and after roof fall is a very important issue for evaluating and forecasting rockburst danger. By experimental tests for combined coal and rock samples rockburst failure and in-situ measurements in a strong rockburst coal mine, the frequency-spectrum evolutionary rule and precursory characters were analyzed in detail. The following conclusions were drawn: (1) Precursory MS signals show the elevated energy and events, lower frequency and trend of spectrum moving to low-frequency band; (2) mainshock signals of rockburst are characterized by maximum amplitude (vibration velocity), wider spectrum, and higher predominant frequency; and (3) aftershock signals are characterized by the sudden decreasing amplitude, highest predominant frequency, and trend of spectrum moving to high-frequency band.

1. Introduction

With the innovation of coal mining process and equipment in China, such as the advanced combined support system, no coal pillar mining technology with reused roadway, and the high-strength and high-resistance hydraulic support equipment application, etc., large-scale and strong-mining working face are possible. However, the ability of the mine disaster prevention and mitigation to adequately characterize the geotechnical environment and keep up with changing geologic conditions severely lags the advance rate of mining equipment and processes. Dynamic stressing produced by key strata strenuous movement and fracture in roof caving zone can trigger easily the strong mining tremor (even rockburst disaster). For example, the working resistance of hydraulic support in a fully mechanized working face of Tashan coal mine (TCM) belong to Datong coal mine group (DCMG) is up to 13,000 kN, but in the period of roof fracture and pressuring, the damaging hydraulic support accidents caused by impact pressure frequently happened. On June 27, 2004, a rockburst disaster was triggered by the overlying hard and thick roof falls nearest mining coal seam in a working face of Muchenjian coal mine (MCM), Beijing coal mine group (BCMG), about 530 m roadway was destroyed, and resulted in 6 fatalities. A 117–136 m thick and hard igneous rock (the uniaxial compressive strength is 102.3–161.9 MPa) covered the main mining seams in Haizi coal mine (HCM) of Huaibei coal mine group (HCMG), and induced many coal and rock dynamic accidents by the mined movement and fracture. On July 17, 2011, an intruded hard igneous rock (the uniaxial tensile strength is up to 35 MPa) fracture in 10414 working face of Yangliu coal mine (YCM) of HCMG caused the strong gas expulsion phenomena in 2# gas suction ground borehole. The severe rockburst disaster triggered by a 180–550 m thick and hard conglomerate rock movement happened in 21221 working face of Qianqiu coal mine (QCM) on November 3, 2011, and caused 8 fatalities in underground and a regional earthquake, which attracted the extensive concern to the society and the central government in China.

As a consequence of the above, the hard and thick roof fall is a severe hazard in mining that can lead to injuries and deaths, damaged equipment, blocked escape routes, and disrupted resource production in coal mines. Predicting roof falls and prevention induced rockbursts can improve mine safety by providing enough forewarning of roof fractures that equipment and

* Corresponding author at: School of Mining Engineering, Key Laboratory of Deep Coal Resource Mining (Ministry of Education), China University of Mining and Technology, Xuzhou, Jiangsu 221116, PR China. Tel.: +86 137 767 834 84.
E-mail address: cplucumt@126.com (C.-P. Lu).

1365-1609/$ - see front matter © 2013 Elsevier Ltd. All rights reserved.
http://dx.doi.org/10.1016/j.ijrmms.2013.08.022

personnel can be moved out of the dangerous area before the strong mining tremor (rockburst) occurs.

The brittle nature of rock fractures often makes it difficult to detect precursor signs of failure with traditional displacement measurements because deformations prior to the onset of significant instability may be very small [1]. Even if rocks have high brittleness and hardly any apparent deformations until failure, the failure process actually begins from an early stage at micro-energy level. Micro-energy level failure is commonly accompanied by increments of deformation that are related to the acoustic emission and microseism (AE&MS) of faint elastic waves. Therefore, it is possible to capture the early precursor signs of failure by monitoring AE&MS signals. The application of the AE/MS system, which monitors self-generated acoustic signals occurring within the ground, has now rapidly increased for monitoring of the stability of underground structures such as mines, tunnels, natural gas, petroleum storage caverns and the extent of the excavation damaged zone (EDZ), as well as surface structures such as foundations, rock, and soil slopes [2].

MS information is able to detect and characterize the rock deformations in a way that is otherwise not possible [3]. As a kind of regional monitoring means, MS system is widely used to monitor and forecast the coal and rock dynamic disasters in coal mines due to its abundant spectrum and wide frequency character, which can monitor surrounding rock fracturing form, roof falls and the released energy of rockburst. The traditional role of MS analysis has been to locate the hypocenter and determine the size of earthquakes or manmade tremors [4]. In metal mines and coal mines of South Africa, the United States, Canada, Poland, France and Germany, earlier and fruitful studies on monitoring the coal and rock dynamic disasters such as rockbursts and mining tremors with MS technology have been conducted.

In the past, most mining-related MS assessments have focused on events such as production blasts from quarries, roof falls, and rock fractures, most of the works are limited to the qualitative assessment, P&S-wave velocity analysis and modeling, as well as accurate source location, etc. For example, Chandlera et al. [5] presented that S-wave velocity information was especially important for purposes of MS hazard modeling. Boadu [6] carried out analytical studies based on a modified displacement discontinuity fracture model to characterize the relations between MS properties and fractured rock mass parameters. Johnson et al. [7] conducted laboratory studies of stick-slip in granular media with and without applied MS vibration, and found dynamic stressing of tectonic faults may play a similar role in determining the complexity of earthquake recurrence. Qin et al. [8] established a dynamical model for modeling the MAE activities in the evolutionary process of the system composed of the stiff hosts (roof and floor) and the coal pillar. Wang et al. [2] improved the MS source location calculation, and put foreword a comprehensive source location approach according to severe roof fall problems in an underground limestone mine. Hazzard et al. [9] presented that a technique was to simulate seismicity in brittle rock under stress using a distinct element numerical PFC modeling code. Bertoncini et al. [10] analyzed the recorded MS monitoring data using classification techniques to predict roof falls in a Pennsylvania limestone mine. Abdul-Wahed et al. [11] established a close correlation between the location of seismic activity and induced stresses in the ground surface of the working areas subjected to rockburst hazards. Murphy et al. [12] correlated the relative radiated seismic energy to the size of the explosion by collecting seismic signatures from underground explosions. Alber et al. [13] described the research on mining-induced seismicity around a specific active longwall at 1100 m depth under several previously mined longwall panels. Young et al. [14] used MS/AE methods for delineating the extent of EDZ, and substantiating the stress modeling. Gudmundsson et al. [15] discussed that the measured MS attenuation is strongly affected by rock fracturing, presence of geothermal fluids there, as well as scattering effects. Brady et al. [16] found that the burst was preceded by a rapid increase of seismic activity, which was followed by a distinct decrease prior to the burst by a moderate rock burst. Shen et al. [17] found that MS and roof stress signals appeared to provide warnings for the imminent roof falls earlier than the roof displacement signals. Iannacchione et al. [18–22] demonstrated a connection between roof rock instabilities and trends in convergence and MS activity, and found that the cumulative frequency based MS criteria were most important in the short forecast windows while the trend based criterion were more important in the longer forecast windows for warning roof falls by monitoring around 200 precursor events relating to roof fracturing before two major roof falls. The National Institute for Occupational Safety and Health (NIOSH) evaluated MS activity from three field sites to compare and contrast the characteristics of MS emissions from very different geologic, stress, and mining environments [3]. The use of MS emissions activity to forecast roof falls has drawn only limited attention, resulting in a lack of published field performance data which supports the use of this technology [21].

The higher static stress in the mining coal material, especially accompanied with the energy input of dynamic stressing wave produced by hard and thick roof falls, easily triggers the stronger rockburst. The acquirement and accurate identification of precursory MS signals is a key issue to predict rockburst danger in coal mines, and the frequency-spectrum characteristics and evolutionary rules of precursory MS signals are regarded as a regional short-term forecasting method. However, little effort has been put towards examining the frequency-spectrum evolutionary rules and the precursory effects of a signature emanating from rockburst based on the experimental tests and in-situ measurements in the deep rockburst mines.

The purpose of this paper is to reveal the MS effects and frequency-spectrum evolutionary rules before, prior to and after rockburst induced by roof falls based on the small-scale combined coal and rock samples deformation and failure experiments and in-situ measurements in a strong rockburst coal mine. By monitoring and analyzing the MS&AE signals in the period of roof fall, the precursory effects and roof fracturing mechanism can be drawn clearly.

2. MS experiment of combined coal and rock rockburst failure

2.1. Experimental system

Experimental system is classified into load device and monitoring apparatus. Load device uses SANS material testing machine which can precisely control load speed, and the load and complete stress–strain curve of coal and rock sample deformation until failure can be recorded. TDS-6MS test apparatus is applied to collect the MS signals produced by combined coal and rock samples deformation and failure, which is composed of 6 substations and a central main station. The predominant frequency band of sensor is 1–100 Hz, and the response frequency for coal and rock deformation is about 1–500 Hz. When Short Term Averaging/Long Term Averaging (STA/LTA) ratio goes above the threshold set, the substation will go into a pre-trigger or trigger mode. Threshold value is a floating point number usually in the range of 1.3–9.0 for TDS-6 system. In this experiment, STA/LTA ratio was set to be 1.5. The scan interval time is 1 s, and the maximum sample voltage value is 5000 mV. When collecting data of more than 4 substations are bigger than the threshold value set simultaneously, the signal

will be recorded from 10 s before the MS event incident and to 30 s after it.

2.2. Combined coal and rock samples process and tests

Real rockburst phenomenon in coal mine is very difficult to simulate actually in the laboratory because of the complicated and incomplete revealed mechanism and the large-scale effect of coal and rock structure. Many researchers have carried out some trials, for example, He et al. [23,24] simulated the impact-induced burst of pure granite and limestone samples by the deep underground rockburst analog testing machine (DURATM) and deep rock non-linear mechanical testing system based on that rockburst induced by blasting or excavation was considered. However, the essence of rockburst is that the stability of the system composed of roof, coal and floor was disturbed and destroyed. Therefore, it is decided that the small-scale combined "roof–coal–floor" samples are applied to test MS signals in the process of deformation, fracturing, and failure by load until bursting in the laboratory, to reveal the precursory effect of rockburst induced by hard roof and floor holding to coal.

Coal was collected from Zhuji coal mine (ZCM) of Huainan coal mining group (HCMG), and rock was collected from Gucheng coal mine (GCM) of Linyi coal mining group (LCMG), where strong rockbursts often happened. The uniaxial and unconfined compressive strength of roof and coal is as high as 122.89 MPa and 7.48 MPa, respectively. Via the standard *ISRM*, coal and rock materials were drilled into samples 50 mm in diameter, sawn into about 20, 30, 40, 50 mm high segments, and then grinded precisely at both ends. Nonparallelism of both ends was required to less than 0.01 mm, and the deviation in diameter was less than 0.02 mm. According to the different height ratio and "roof–coal–floor" combined mode, the cylinder segments were stuck into nearly 50×100 mm^2 standard samples using AB strong glue, and the total is 11. Fig. 1 shows the photographs of combined coal and rock samples and sublayer structure. Table 1 shows the samples height and each sublayer height ratio.

In this experiment, the uniaxial cyclic loading and unloading mode was used. Firstly, the loading rate was 0.2 kN/s until 5 kN, and then unloading to 0.2 kN, after that, loading again until sample rockburst failure completely. Simultaneously, the MS signals were recorded in the whole period of sample deformation, fracture and rockburst failure. 4 sensors of TDS-6MS system were arranged near the being tested sample. In which, two were placed on the load-bearing plate of test machine, one was placed on the load plate, and the last was placed on the ground near the test machine base. Main measured parameters included the amplitude (mV), the vibration acceleration (cm/s^2), and duration (ms) of MS signals, etc.

Generally, once fracture in sample, stress will decrease, the MS signal will be generated, which can be captured by sensors. When coal or rock segment of combined samples is broken completely, the load of test machine does not continue to rise. At this time, rockburst failure of sample can be verified, and the acquisition of MS signal will stop.

2.3. Analysis on MS frequency-spectrum evolution

In this experiment, when coal and rock deformation, fracture and rockburst failure, the MS signals (Strictly speaking, acoustic emission) will propagate and attenuate through coal and rock medium, test machine, as well as machine base, after a great degree of attenuation, the residual MS signals will be recorded by TDS-6 system. Therefore, the real measured signals have the low-frequency and low-amplitude characteristics.

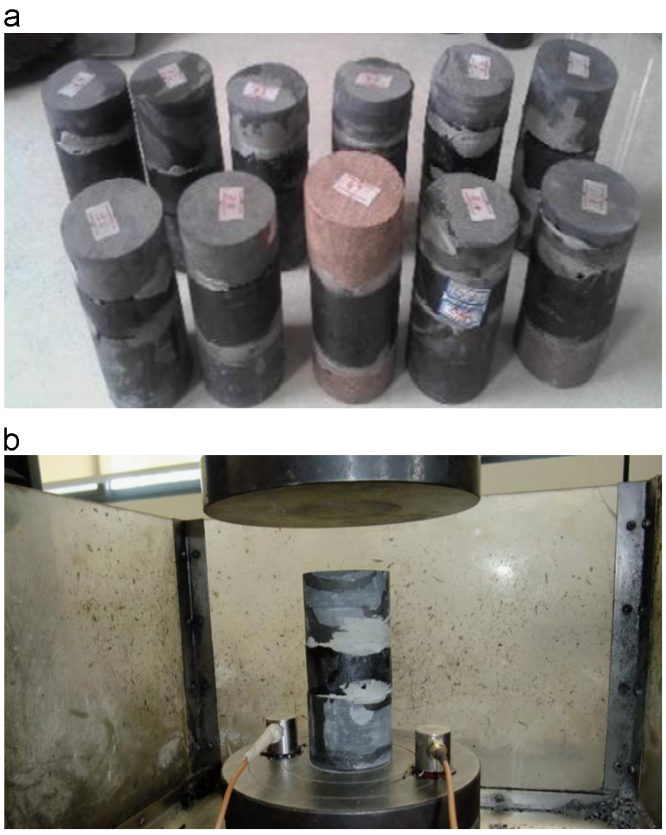

Fig. 1. Photographs of combined coal and rock samples and sublayer structure. (a) Combined coal and rock samples. (b) Sublayer structure of roof–coal–floor.

Table 1
Samples height and each sublayer height ratio. Note: R—roof; C—coal; F—floor.

Sample label	Sample height (mm)	Sublayer height ratio (R:C:F)
RCF1	104	1.48:2.48:1
RCF2	105	1.39:1:1.36
RCF3	97	2.74:1.37:1
RCF4	104	2.22:1.3:1
RCF5	99	1.95:1.55:1
RCF6	96	2.36:1:1
RCF7	98	1.46:1:1.01
RCF8	97	1.82:1.59:1
RCF9	104	1:2.36:1.36
RCF10	94	3.25:1.63:1
RCF11	95	1.45:2.3:1

The original MS signals will contain the noise produced by the test machine running. Take into account the central frequency of noise is about 50 Hz, which can be removed by the band-stop filter method. For the accurate frequency-spectrum analysis, all signals were de-noised by the band-stop filter, and analyzed by the Fourier transform, which was one of the most commonly used methods for signal processing. The Fast Fourier Transform (FFT) converted a signal from the time dependent into the frequency dependent and provided a very convenient and efficient means for MS signal processing.

Figs. 2–5 show the amplitude–time and amplitude spectrum–frequency distribution curves of foreshock, mainshock and aftershock signals collected in the process of deformation, fracturing and rockburst failure of combined coal and rock samples, and the double logarithmic coordinates (the horizontal coordinate logarithmic scale=2, and the vertical coordinate logarithmic scale=10) were adopted in Figs. 2–5(b). Based on paper length restriction, only

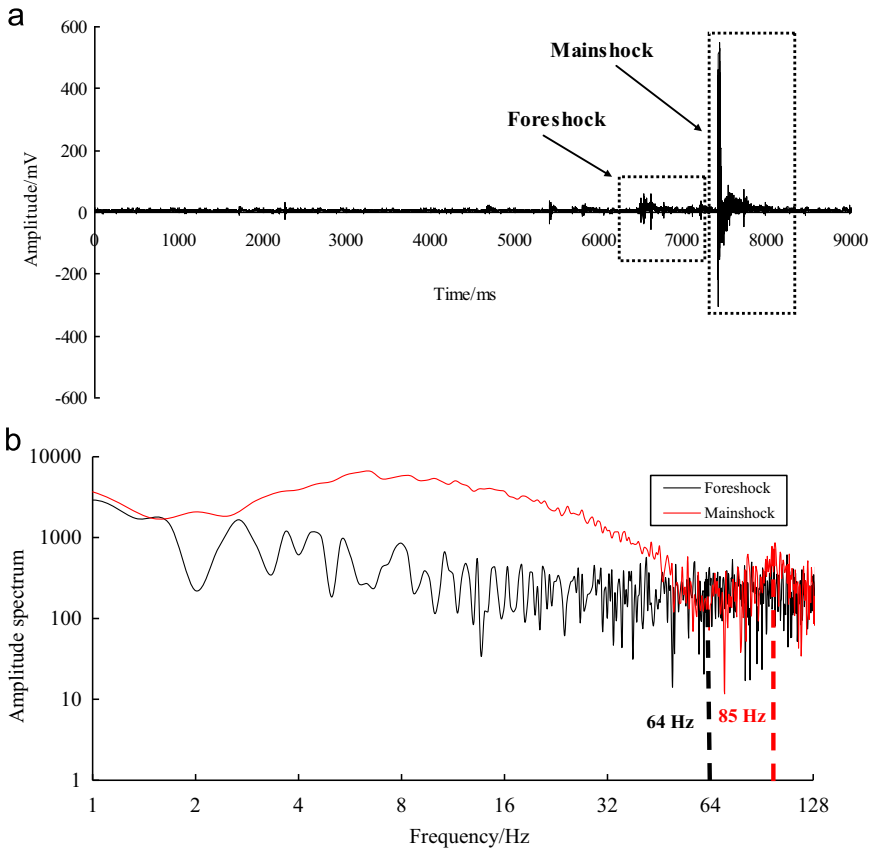

Fig. 2. Foreshock and mainshock signals collected from RCF7 sample. (a) Amplitude–time. (b) Amplitude spectrum–frequency.

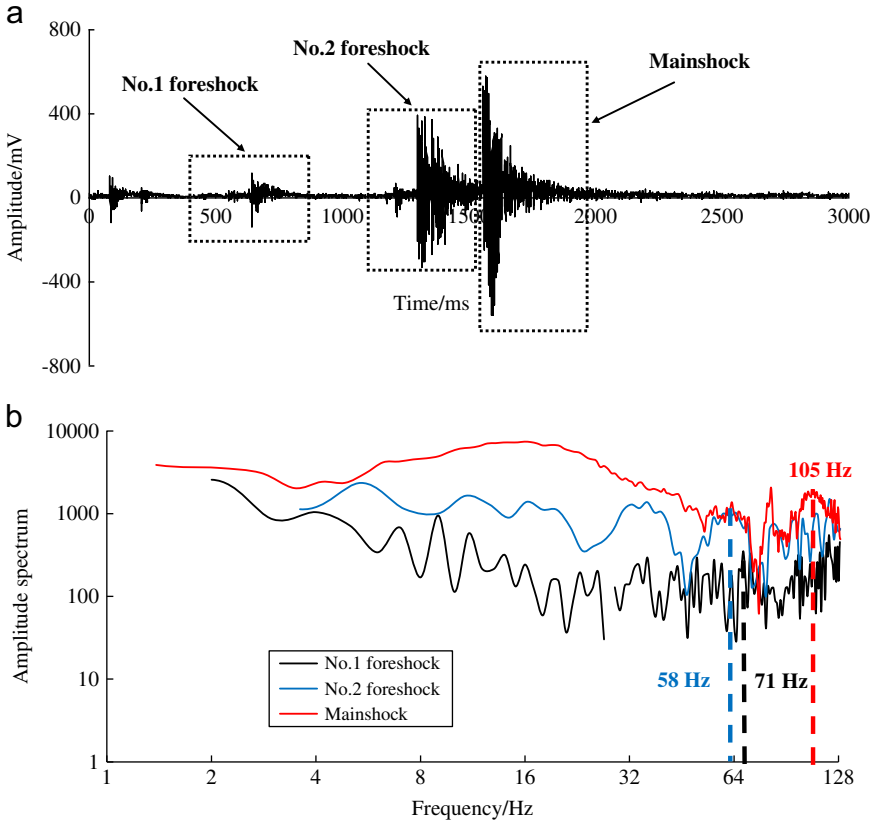

Fig. 3. Foreshock and mainshock signals collected from RCF9 sample. (a) Amplitude–time. (b) Amplitude spectrum–frequency.

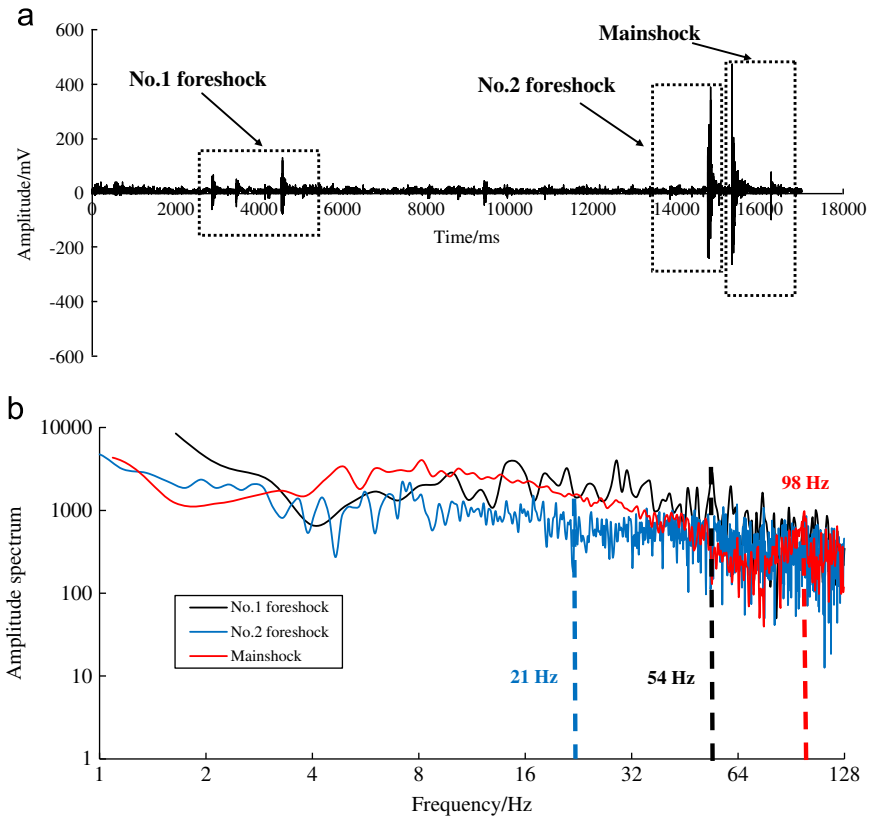

Fig. 4. Foreshock and mainshock signals collected from RCF11 sample. (a) Amplitude–time. (b) Amplitude spectrum–frequency.

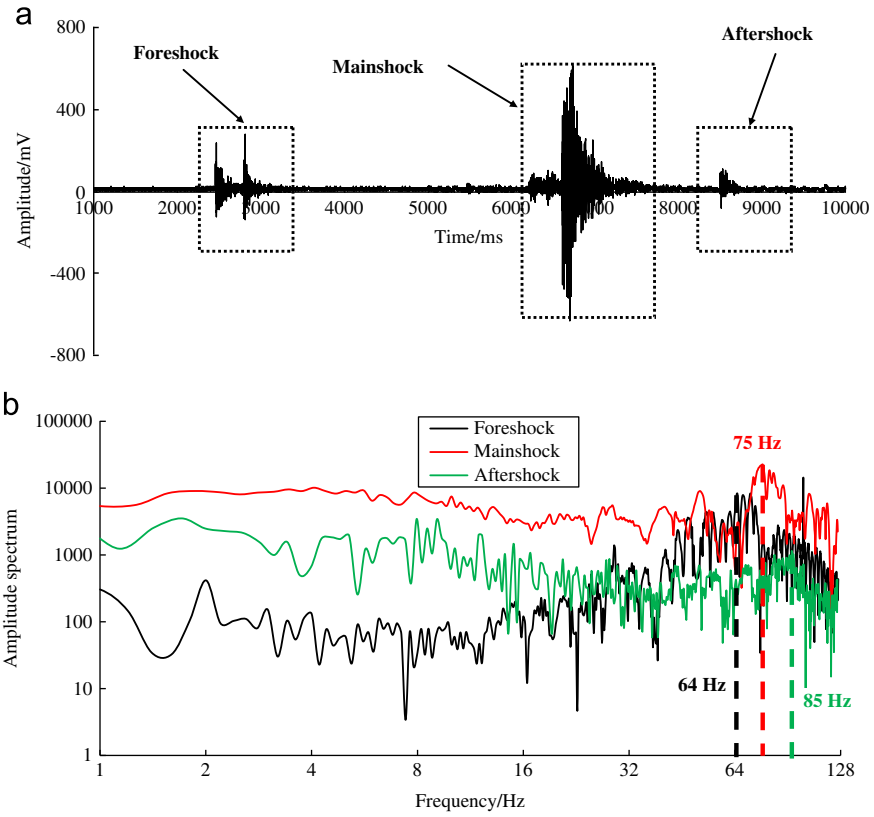

Fig. 5. Foreshock, mainshock and aftershock signals collected from RCF4 sample. (a) Amplitude–time. (b) Amplitude spectrum–frequency.

one substation MS results of the representative samples (RCF4, RCF7, RCF9 and RCF11) were analyzed in detail.

According to the frequency spectrum distribution characteristics of foreshock, mainshock and aftershock signals, the following conclusions can be drawn. (i) Prior to rockburst failure of combined coal and rock samples, the frequency spectrum of MS signals began to move to low-frequency band, especially for multiple precursory signals. For example, in Figs. 3 and 4(b), as rockburst failure approached, the precursory signals showed the gradual increasing amplitude and decreasing predominant frequency. The low-frequency components of mainshock signals increased significantly, while the predominant frequency was higher compared with the precursory signals. Simultaneously, the high-frequency components also enhanced obviously. Amplitude spectrum of aftershock signal weakened obviously, and the predominant frequency moved to high-frequency band compared with mainshock signal. (ii) Bursting energy index (BEI) is the ratio of the stored deformation energy before stress peak to the dissipated deformation energy after stress peak, which can be accurately calculated based on the complete stress–strain curve of coal and rock sample under the uniaxial compressive load. BEI can reflect rockburst failure intensity of sample. The measured BEI values of samples RCF7、RCF9 and RCF11 were 1.576, 0.505 and 0.794, respectively, and the corresponding predominant frequency of mainshock signals of three samples were 85 Hz, 105 Hz and 98 Hz, which indicated that there was a negative relationship between predominant frequency of mainshock signal and rockburst failure intensity of sample. (iii) Based on the frequency-spectrum distributions of foreshock, mainshock and aftershock signals in the complete process of deformation, fracture and bursting failure of combined coal and rock samples (Fig.5 (b)), the predominant frequency of foreshock, mainshock and aftershock signals were 64 Hz, 75 Hz and 85 Hz, respectively. It can be deduced that the frequency-spectrum evolutionary rule characterized: lower amplitude and frequency, frequency spectrum moving to high-frequency band→peak amplitude value, and higher predominant frequency→the sudden decreasing amplitude spectrum, and highest predominant frequency.

3. Case study in Huating coal mine

3.1. Introduction of 250103 working face

250103 is the third working face of 2501 mining district of Huating coal mine (HCM), which is mining the top first sublayer (13.2 m) of 5# coal seam. The average thickness of 5# coal seam is 36 m, and the average angle is 5°–8°. The maximum mining depth is 791 m, and the original in situ vertical stress is about 19.8 MPa. The strike and sloping length of 250103 working face is about 2336 m, and 213.3 m, respectively. The south boundary of 250103 working face is the protective pillar of the main roadway of 2501 mining district, the

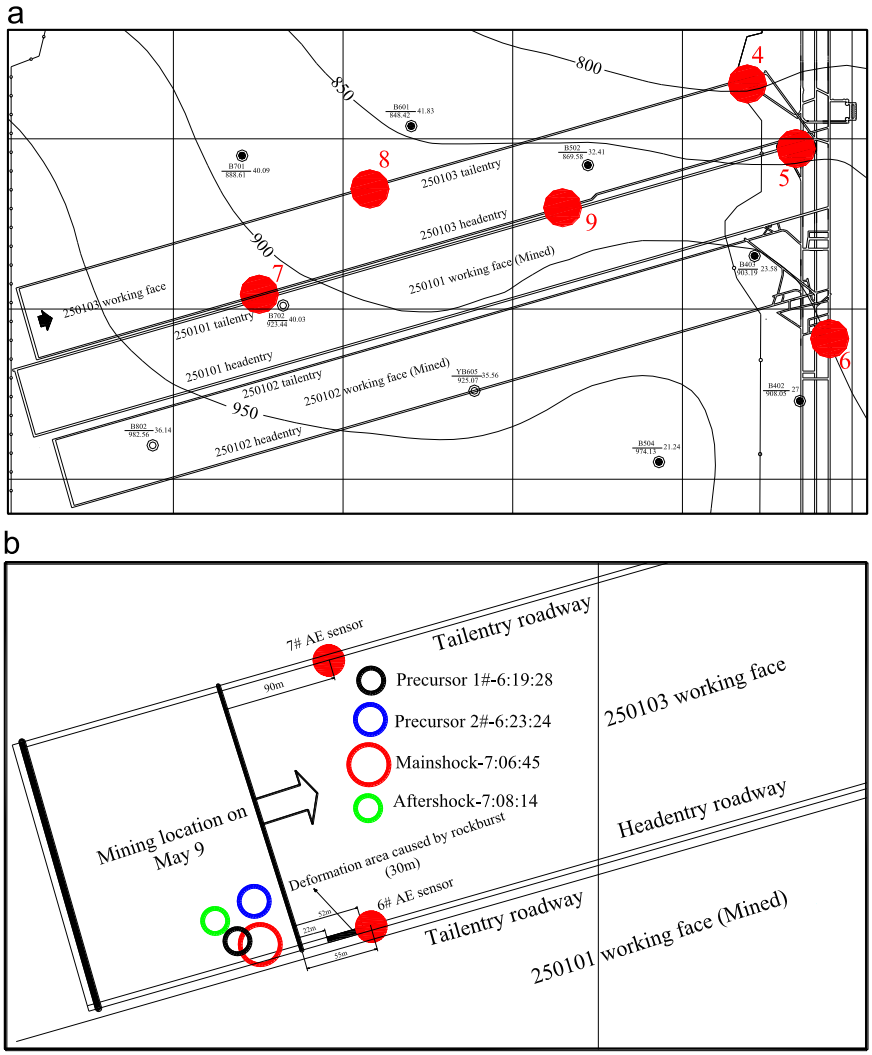

Fig. 6. The plane sketch of 250103 working face, source locations, and MS&AE sensors arrangement. (a) 250103 working face and 4#–9# MS sensors arrangement. (b) Source locations, rockburst damaging area and AE sensors arrangement.

north boundary is the protective pillar of the north-wing main roadway of the second mining level of adjacent Yanbei coal mine (YCM), the west boundary is the protective pillar of 250101 working face tailentry, and the east boundary is the unexcavated coal material. Fig. 6 shows the plane sketch of 250103 working face, source locations and MS&AE sensors arrangement.

The primary roof of 250103 working face is dark gray siltstone, and its thickness is generally 20–25 m. The immediate roof is mainly gray silty-mudstone, and its thickness is 6–9 m. The immediate floor is mainly gray and black mudstone, and its thickness is 0.5–2.1 m. The primary floor is gray gritstone, and its thickness is generally 12–19 m. Table 2 shows the properties of roof and floor of 5# coal seam.

From March 2, 2010 (the beginning mining date) to June 7, 2011, the total 83 strong mining tremor events happened in 250103 working face, which led to 9 injuries, and influenced severely the production, safety and the mining speed.

3.2. SOS MS and ARES-5/E AE monitoring system

To detect the overlying roof fracturing and falls, especially forecast the rockburst danger of 250103 working face in time, SOS MS monitoring system, developed by Poland Central Mining Institute, was installed in 2007, which is composed of real-time monitoring recorder, analyzer, sensors and the digital transmission system, etc. The frequency range of sensor is 1–600 Hz, the sampling rate is 500 Hz, A/D converter is 16 bits, and the maximum data transmission rate is 1 MB/s. The system can immediately, continuously, and automatically collect and filter shock signals, and accurately calculate the occurrence time, energy and three-dimensional coordinates of shock event ($E > 100$ J) using Powell location algorithm. The constant velocity model is proposed for location, which is calibrated by time residual error of arrival of a number of large shock signals. The sensor is designed to broadband and moving-coil type speed sensor, the resonance frequency is 4.5 ± 0.75 Hz, the response of which is flatted by filter, and the cable noise can be eliminated through 50 Hz band-pass filter of the controllable switch. Before arranging the sensors, we have achieved the positioning error limits that were desired by two objective functions of minimum arrival time residuals and minimum source location errors, created under two conditions with strong tremor signals only and also mixed with blasting signals. These objective functions were solved by the mixed algorithm combining genetic algorithm with CMEAS algorithm.

The three-dimensional monitoring pattern used sixteen sensors, of which fifteen were installed in the underground roadways, and one was arranged on surface bedrock. 250103 working face was surrounded by the total five sensors (4#, 5#, 7#, 8# and 9#, correspondingly) (Seen from Fig. 6(a)). Table 3 shows the three-dimensional coordinates of sixteen sensors. The elevation of 250103 working face is 828.93–998.05 m, and the corresponding ground elevation is 1457–1620 m.

ARES-5/E system mainly consists of ground central station, SP-5.28/E sensor, N/TSA-5.28/E transmitter and the digital transmission system, etc. Generally, the system provides eight AE sensors. The signal transmission distance is less than 10 km. The frequency arrange of sensor is 28–1500 Hz, and the maximum sampling frequency is 10 kHz.

For the continuous and real-time monitoring of small energy AE events in 250103 working face, ARES-5/E system was installed in HCM on May 25, 2008, and operated normally on May 30. The total of eight sensors were arranged, in which, 5# and 6# were installed in roof of 250103 working face headentry, and 7# and 8# were installed in Tailentry. According to the actual data in the field, the sensor can record AE event count and energy a minute. To reveal overlying key stratum fracturing and fall laws along with mining using AE monitoring, the daily average event count and energy were calculated and analyzed. On May 9, 6# sensor was 54.6 m away from the cut of working face, and 7# sensor was 90.5 m away from the cut (Seen from Fig. 6(b)).

3.3. Description of rockburst accident

On May 9, 2010, a rockburst accident happened in the advanced support segment of 250103 working face headentry at 7:06 AM, which was caused by the higher and static vertical stress formed in the section coal pillar between 250101 and 250103 working faces and the dynamic stress wave disturbance produced by primary roof fracturing and fall in gob. The total 30 m long roadway between 22 m and 52 m away from the cut of working face was destroyed seriously, which obviously characterized floor heave (the average heave amount was 0.8 m). The major of advanced support individual hydraulic props inclined severely to the coal wall side in headentry. The calculated energy of rockburst mainshock was about 2.2×10^7 J. The located source was 32 m behind cut of 250103 working face in the strike direction, 9.4 m away from the inside wall of headentry in the sloping direction, and in the primary roof stratum in the vertical direction. The locations of precursor, mainshock and aftershock signals of the rockburst marked in Fig. 6(b).

Table 3
The three-dimensional coordinates of 16 sensors.

Sensor number	x (m)	y (m)	z (m)
1	−3900369.72	36378364.26	838.00
2	−3901337.21	36378240.71	837.83
3	−3901132.47	36377757.07	838.66
4	−3901301.83	36376661.47	829.72
5	−3901164.68	36376471.20	860.88
6	−3901065.93	36375912.54	903.11
7	−3901703.83	36375653.42	983.74
8	−3903248.23	36375414.47	1028.34
9	−3902289.04	36375689.52	970.00
10	−3900150.19	36378889.70	1410.70
11	−3903578.96	36375550.68	1044.15
12	−3903593.76	36376582.16	979.66
13	−3901751.44	36375177.71	1477.71
14	−3903468.96	36377440.26	860.65
15	−3901374.29	36378573.20	1071.95
16	−3903102.69	36375256.47	1029.13

Table 2
Properties of roof and floor of 5# coal seam.

Roof and floor	Lithology	Thickness (m)	Property
Primary roof	Dark gray siltstone	20–25	Cemented, developed bedding
Immediate roof	Gray silty-mudstone	12–18	Obvious bedding
False roof	Mudstone	0.3–0.5	Soft and fragile
Immediate floor	Gray and black mudstone	0.5–2.1	Soft, rich carbonaceous
Primary floor	Gray gritstone	12–19	Coarse

3.4. MS&AE monitoring results and analysis

Main purpose of this research is to reveal the MS frequency-spectrum evolutionary law of rockburst induced by roof fall, especially the precursory signal characteristics, which should be closest to the mainshock time and located in roof layer. All other typical mining events prior to the rockburst were eliminated. According to the above requirements, before rockburst, we monitored 41MS events (from 1:36 AM to 6:23 AM on May 9). Taking into account the efficiency and necessity of MS precursory signals

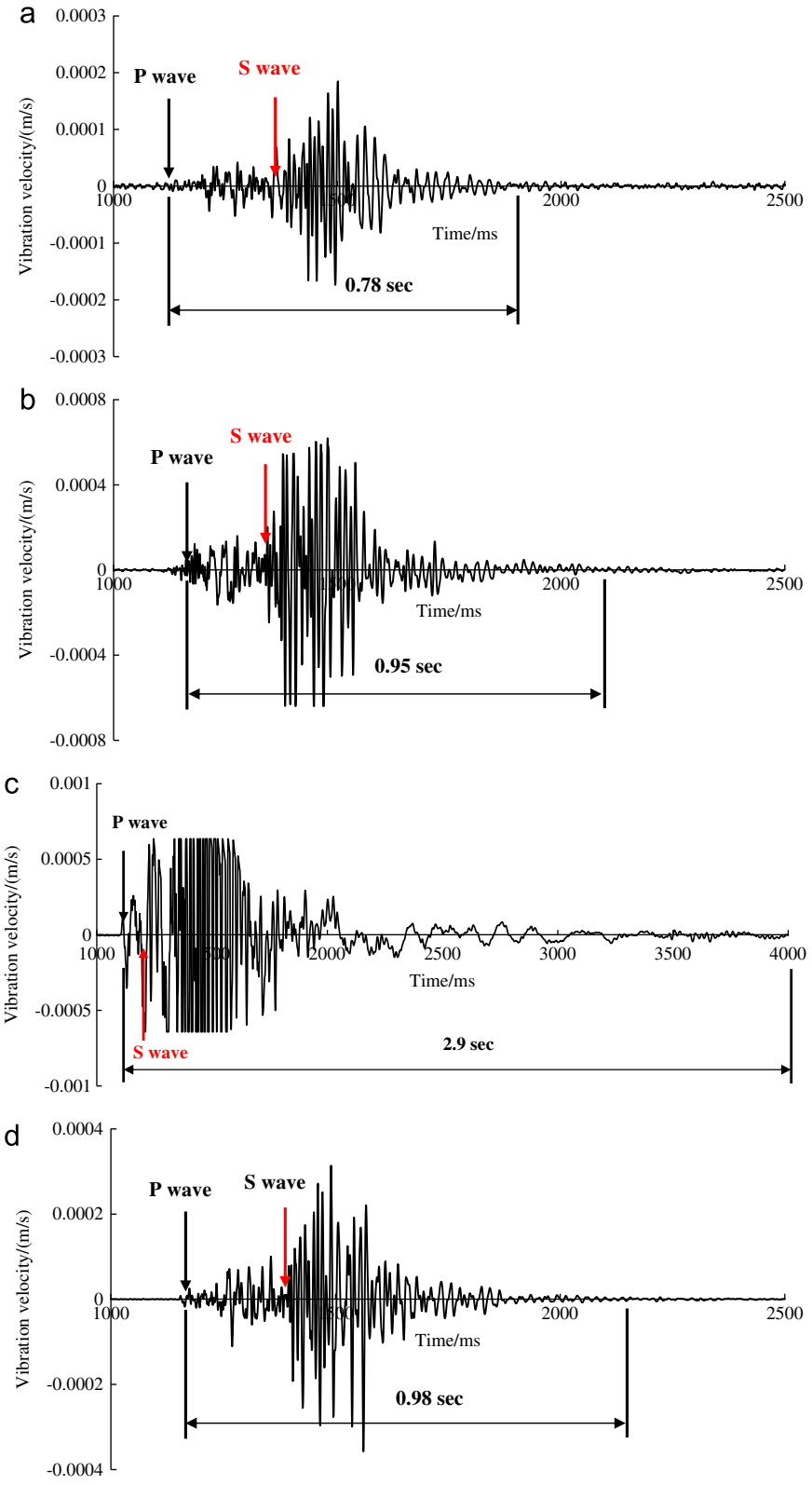

Fig. 7. Vibration velocity–time curves of precursor, mainshock and aftershock signals collected by 7# sensor closest to source center. (a) 1# precursor signal recorded at 06:19:28. (b) 2# precursor signal recorded at 06:23:24. (c) Mainshock signal recorded at 07:06:45. (d) Aftershock signal recorded at 07:08:14.

analysis, we chose two events closest to the mainshock to reflect the characteristics of roof fall. Two precursory signals were recorded at 6:19:28 and 6:23:24, and mainshock and aftershock signals were recorded at 7:06:45 and 7:08:14, respectively. Fig. 7 shows the vibration velocity–time curves of precursor, mainshock and aftershock signals collected by 7# sensor closest to source center.

From Fig. 7, it is known that vibration velocity of precursor signals gradually increased from 1.85×10^{-4} m/s to 6.19×10^{-4} m/s prior to rockburst, which indicated that roof fracturing intensity obviously enhanced. According to waveform characteristics of mainshock signal when rockburst [25], it can be verified that it was a typical MS signal generated by roof fall. By identification of small roof falls prior to the larger impact event recorded by the MS system, impact events differ from fracture events in that they are emergent wave forms that are often several seconds in duration [19]. Another, the first half of mainshock waveform characterized the higher frequency and amplitude, and the second half appeared the lower frequency and decreasing amplitude. Overall, the mainshock signal showed the broadband characteristics. The high-frequency part of mainshock waveform indicated that a large number of micro-cracks were being generated inside primary roof stratum, subsequently, began to converge, connect and form macro-fracture surface, and then the low-frequency part was produced. Finally, the rockburst was triggered. After that, the intensity of aftershock signal reduced significantly.

For most shock signals, the low-frequency component is usually the most important part, which can manifest the main features of the signals, while the high-frequency component generally is associated with noise and disturbances, and if the high-frequency part of the signal is removed carefully, the signal key characteristics can still be retained. Based on SOS MS system can automatically filter shock signal and the waveform character produced by roof fall is considered, the rockburst signals do not need special process. Taking into vibration wave propagation and attenuation laws account, to reveal frequency-spectrum evolutionary rule of roof fall, the signals recorded by 7# and 8# sensors closest to the source center were analyzed in detail. Figs. 8 and 9 show the amplitude spectrum–frequency distribution curves of precursor, mainshock and aftershock signals recorded by 7# and 8# sensors, respectively, and the double logarithmic coordinates (the horizontal coordinate logarithmic scale=5, and the vertical coordinate logarithmic scale=10) were adopted.

From Fig. 8, prior to rockburst, the amplitude spectrum of precursor signals gradually enhanced, especially in the low-frequency band (<25 Hz), and the predominant frequency values were 25 Hz and 38 Hz, respectively. When rockburst occurred, the amplitude spectrum of mainshock signal reached peak value in the low-frequency band (<50 Hz), and the low-frequency components enhanced significantly. After rockburst, the amplitude spectrum of aftershock signal suddenly and sharply decreased compared with mainshock signal, the spectrum moved to the high-frequency band, and the predominant frequency was 50 Hz. According to Fig. 9, the similar conclusions can also be drawn. However, the propagation distance of MS signal recorded by 8# sensor was larger than it recorded by 7# sensor. According to the propagation and

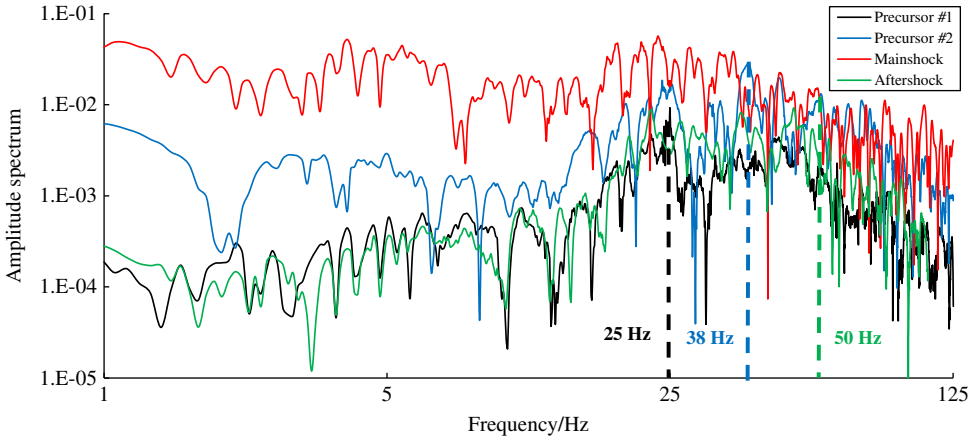

Fig. 8. Amplitude spectrum–frequency curves of precursor, mainshock and aftershock signals recorded by 7# sensor.

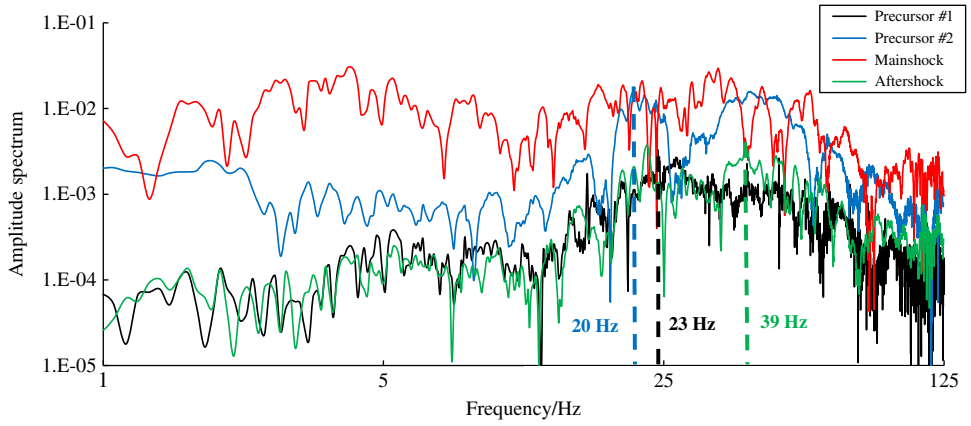

Fig. 9. Amplitude spectrum–frequency curves of precursor, mainshock and aftershock signals recorded by 8# sensor.

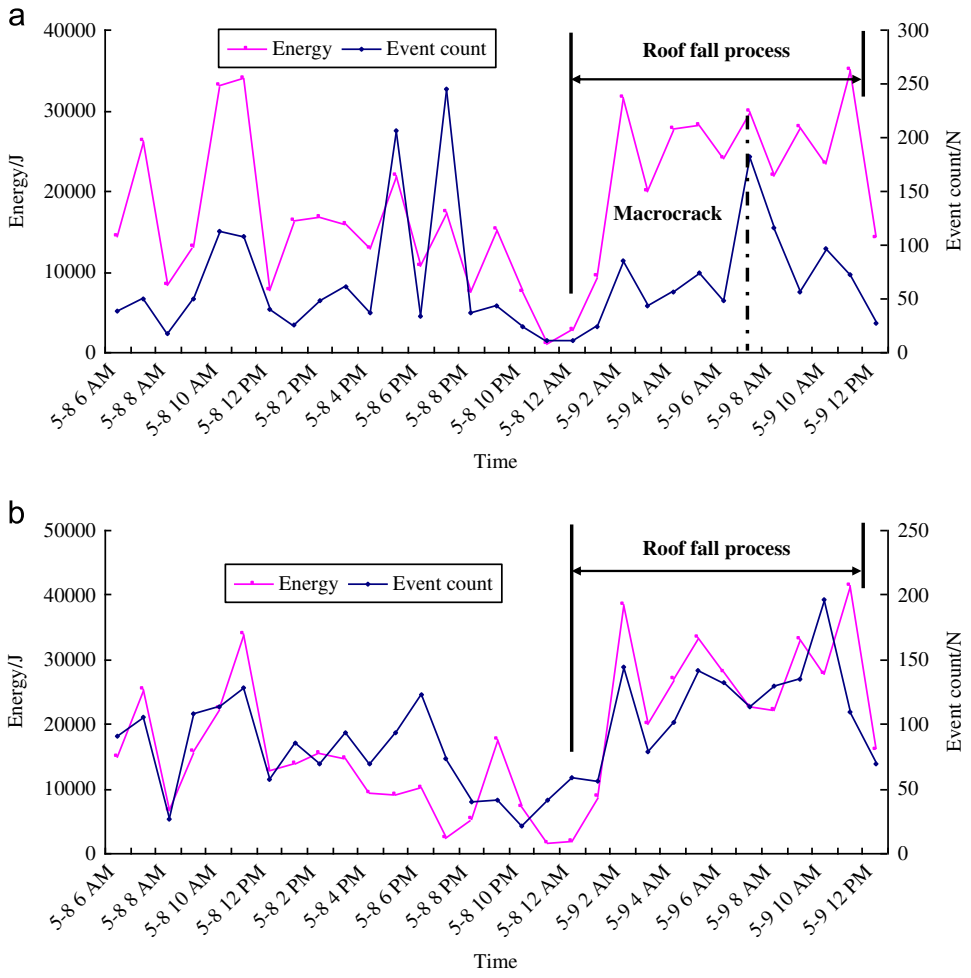

Fig. 10. Energy and event count–time curves of AE signals in the process of roof fall. (a) AE signal recorded by 6# sensor. (b) AE signal recorded by 7# sensor.

attenuation laws of shock wave [26,27], the larger the distance between sensor and roof fall source is, the weaker the intensity of signal is, and the lower the frequency of signal is, especially for the high frequency signal. Therefore, the predominant frequency (20 Hz and 23 Hz) of precursor signals and the predominant frequency (39 Hz) of aftershock signal collected by 8# sensor were lower than it collected by 7# sensor.

Fig. 10 shows the energy and event count–time curves monitored by 6# and 7# AE sensor every 1 h in the process of roof fall. It can be known that roof fall period was about from 12 AM on May 8 to 11 AM on May 9. According to the macro-effect of AE signals, before roof fall, the energy and event count sharply increased. In the period of roof fall, the energy and event count stayed at a higher level, after that, suddenly deceased. Because 6# sensor was close to rockburst source location, it can effectively reveal the characteristics of roof fall. From Fig. 10(a), before 7 AM on May 9, the event count increased dramatically, reached peak (the value was 182) at 7 AM, and then suddenly decreased, which indicated that the macrocrack time of roof fall was about at 7 AM. The conclusion is strictly consistent with the analysis of MS monitoring results.

4. Conclusions

(1) Prior to the rockburst induced by roof fall, the precursor MS signals showed the gradual increasing amplitude and decreasing predominant frequency. The low-frequency components of mainshock signals increased significantly, while the predominant frequency was higher. Amplitude of aftershock signal weakened obviously, and the predominant frequency moved to high-frequency band.

(2) There was a negative relationship between predominant frequency of mainshock signal and rockburst failure intensity.

(3) MS frequency-spectrum evolutionary rule characterized: lower amplitude and frequency, frequency spectrum moving to high-frequency band→peak amplitude value, and higher predominant frequency→the sudden decreasing amplitude spectrum, and highest predominant frequency.

(4) Before roof fall, the AE energy and event count sharply increased. In the period of roof fall, the energy and event count stayed at a higher level, after that, suddenly deceased.

Acknowledgments

The authors wish to express their thanks to the collaborative funding support from the Fundamental Research Funds for the Central Universities (2013RC03), the Program for Innovative Research Team in University (IRT1084), the Project Funded by the Priority Academic Program Development of Jiangsu Higher Education Institutions (SZBF2011-6-B35), and the Jiangsu Overseas Research & Training Program for University Prominent Young & Middle-aged Teachers and Presidents. In particular we wish to thank Liu Shi-min, Liu Biao and Du Binbin for their contributions to this research.

References

[1] Cheon DS, Jung YB, Park ES, et al. Evaluation of damage level for rock slopes using acoustic emission technique with waveguides. Engineering Geology 2011;121:75–88.

[2] Wang HL, Ge MC. Acoustic emission/microseismic source location analysis for a limestone mine exhibiting high horizontal stresses. International Journal of Rock Mechanics and Mining Sciences 2008;45:720–8.

[3] Iannacchione AT, Prosser LJ, Grau R, et al. Roof monitoring helps prevent injuries in stone mines. Minerals Engineering 2000;52:32–7.

[4] Ellenberger J., Bajpayee T. An evaluation of microseismic activity associated with major roof falls in a limestone mine: a case study. In: Proceedings of the 2007 Society for mining, metallurgy, and exploration annual meeting and exhibit. Denver; 25–28 February 2007. p. 1–5.

[5] Chandler AM, Lam NTK, Tsang HH. Shear wave velocity modelling in crustal rock for seismic hazard analysis. Soil Dynamics and Earthquake Engineering 2005;25:167–85.

[6] Boadu FK. Fractured rock mass characterization parameters and seismic properties: analytical studies. Journal of Applied Geophysics 1997;36:1–19.

[7] Johnson PA, Savage H, Knuth M, et al. Effects of acoustic waves on stick-slip in granular media and implications for earthquakes. Nature 2008;451:57–60.

[8] Qin SQ, Jiao JJ, Tang CA, et al. Instability leading to coal bumps and nonlinear evolutionary mechanisms for a coal–pillar–roof system. International Journal of Solids and Structures 2006;43:7407–23.

[9] Hazzard JF, Young RP. Dynamic modelling of induced seismicity. International Journal of Rock Mechanics and Mining Sciences 2004;41:1365–76.

[10] Bertoncini CA, Hinders MK. Fuzzy classification of roof fall predictors in microseismic monitoring. Measurement 2010;43:1690–701.

[11] Abdul-Wahed MK, Heib MA, Senfaute G. Mining-induced seismicity: seismic measurement using multiplet approach and numerical modeling. International Journal of Coal Geology 2006;66:137–47.

[12] Murphy MM, Westman EC, Iannacchione AT, et al. Relationship between radiated seismic energy and explosive pressure for controlled methane and coal dust explosions in an underground mine. Tunnelling and Underground Space Technology 2012;28:278–86.

[13] Alber M, Fritschen R, Bischoff M, et al. Rock mechanical investigations of seismic events in a deep longwall coal mine. International Journal of Rock Mechanics and Mining Sciences 2009;46:408–20.

[14] Young RP, Collins DS. Seismic studies of rock fracture at the underground research laboratory, Canada. International Journal of Rock Mechanics and Mining Sciences 2001;38:787–99.

[15] Gudmundsson O, Finlayson DM, Itikarai I, et al. Seismic attenuation at Rabaul volcano, Papua New Guinea. Journal of Volcanology and Geothermal Research 2004;130:77–92.

[16] Brady BT, Leighton FW. Seismicity anomaly prior to a moderate rock burst: a case study. International Journal of Rock Mechanics 1977;14:127–32.

[17] Shen B, King A, Guo H. Displacement, stress and seismicity in roadway roofs during mining-induced failure. International Journal of Rock Mechanics and Mining Sciences 2008;45:672–88.

[18] Iannacchione AT, Coyle PR, Prosser LJ, et al. The relationship of roof movement and strata induced microseismic emissions to roof falls. Minerals Engineering 2004;56:53–60.

[19] Iannacchione A.T., Burke L.M., Chapman M.C. Characterizing roof fall signatures from underground mines. In: Proceedings of the 6th international symposium on rockburst and seismicity in mines. Perth; 9–11 March 2005. p. 619–29.

[20] Iannacchione A.T., Esterhuizen G.S., Bajpayee T.S., et al. Characteristics of mining-induced seismicity associated with roof falls and roof caving events. In: Proceedings of the 40th US rock mechanics symposium. Anchorage; 27–29 June 2005. p. 10–19.

[21] Iannacchione A.T., Bajpayee T.S. Forecasting roof falls with monitoring technologies – a look at the Moonee colliery experience. In: Proceedings of the 24th international conference on ground control in mining. Morgantown; 2–4 August 2005. p. 44–51.

[22] Iannacchione A.T., Batchler T., Marshall T.E. Mapping hazards with microseismic technology to anticipate roof falls – a case study. In: Proceedings of the 23rd international conference on ground control in mining. Morgantown; 3–5 August 2004. p. 327–33.

[23] He MC, Miao JL, Feng JL. Rock burst process of limestone and its acoustic emission characteristics under true-triaxial unloading conditions. International Journal of Rock Mechanics and Mining Sciences 2010;47:286–98.

[24] He MC, Miao JL, Li DJ, et al. Experimental study on rockburst processes of granite specimen at great depth. Chinese Journal of Rock Mechanics and Engineering 2007;26:865–76.

[25] Mu Z.L. Study on the burst-energy principle of rock burst induced by roof stratum and its application. [Ph.D. thesis]. Xuzhou, Jiangsu: China University of Mining and Technology; 2007.

[26] Lu CP, Dou LM, Wu XR, et al. Case study of blast-induced shock wave propagation in coal and rock. International Journal of Rock Mechanics and Mining Sciences 2010;47:1046–54.

[27] Lu CP, Dou LM, Liu H, et al. Case study on microseismic effect of coal and gas outburst process. International Journal of Rock Mechanics and Mining Sciences 2012;53:101–10.